PAPER

A simple way to achieve superhydrophobicity, controllable water adhesion, anisotropic sliding, and anisotropic wetting based on femtosecond-laser-induced line-patterned surfaces†

Jiale Yong, Qing Yang, Feng Chen,* Dongshi Zhang, Umar Farooq, Guangqing Du and Xun Hou

The superhydrophobicity, controllable water adhesion, anisotropic sliding, and anisotropic wetting, which are four typical aspects of the wettability of solid surfaces, have attracted much interest in fundamental research and practical applications. However, how to use a simple and effective method to realize all those properties is still a huge challenge. Here, we present a method to realize periodic line-patterned polydimethylsiloxane (PDMS) surfaces by a femtosecond laser simply and efficiently. By adjusting the period (*D*) or average distance of adjacent microgrooves, the as-prepared surfaces can exhibit superhydrophobicity, controllable water adhesion, anisotropic sliding, and anisotropic wetting. We believe that these multifunctional surfaces have enormous potential applications in novel microfluidic devices, microdroplet manipulation, liquid microdroplet directional transfer, and lab-on-chips.

1 Introduction

Wettability is a very important property of solid surfaces that is governed by both the geometrical microstructure and the chemical composition of the surface.[1–9] In recent years, super-hydrophobicity,[10–14] controllable water adhesion,[15–22] anisotropic sliding,[23–26] and anisotropic wetting,[27–33] which are four typical aspects of wettability, have attracted much interest because of their importance in fundamental research, practical applications, and inspired mimetic attempts. A superhydrophobic surface, displaying a water contact angle (CA) greater than 150°, is initially observed from natural materials such as lotus leaf.[34] The lotus leaf exhibiting superhydrophobicity with ultralow water adhesion is demonstrated as the ideal water-repellent surface. Water droplets on this surface can easily roll off to remove contaminants from the surfaces if the substrate is slightly tilted. This phenomenon is well-known as self-cleaning effect.[34] Such superhydrophobic surfaces have been widely used in many fields, for instance, in the areas of surface self-cleaning, marine coating, preventing the adhesion of snow, fog and raindrops to window surfaces and reducing flow resistance in microfluidic channels.[35–41] On the contrary, a new kind of sticky superhydrophobic surfaces showing ultrahigh water adhesion

like rose petal has recently been reported.[42] On this surface, the CA of the water droplet is usually above 150°, while the water droplet would be stuck and would not roll off even with the surface vertical or upside down. The high-adhesion super-hydrophobic surfaces can provide some fascinating applications in manipulating liquids at the micrometer scale.[43–45] Among these two extreme superhydrophobicites (ultralow water adhesion and ultrahigh water adhesion), recently, superhydrophobic surfaces with controllable adhesion have attracted tremendous scientific interest due to their important applications in many fields, such as biochemical separation, transport of micro-droplets, tissue engineering, and microfluidic chips.[15–22]

In nature, it is well known that the sliding angle (SA) values are different for a water droplet rolling along two vertical directions on the surface of a rice leaf, namely anisotropic sliding.[23,46] This unique property is based on the arrangement of the microstructures of the rice leaf. The microscale papillas are arranged in one-dimensional order parallel to the leaf edge and randomly in the other directions. The anisotropic sliding ability is crucial for water droplets to move along the leaf veins and finally to the root, helping the plants to survive. As another anisotropic phenomenon, anisotropic wetting involves water CA variations along different directions, resulting in an elongated droplet.[27–33] The anisotropic sliding and anisotropic wetting effect can find many applications in liquid manipulation for microfluidics and lab-on-chips.[47–52]

The superhydrophobicity and anisotropic wetting are static characteristics, whereas the controllable water adhesion and anisotropic sliding indicate dynamic features. So far, many

State Key Laboratory for Manufacturing System Engineering & Key Laboratory of Photonics Technology for Information of Shaanxi Province, School of Electronics & Information Engineering, Xi'an Jiaotong University, Xi'an, 710049, P.R. China. E-mail: chenfeng@mail.xjtu.edu.cn

This journal is © The Royal Society of Chemistry 2014

J. Mater. Chem. A, 2014, **2**, 5499–5507 | 5499

techniques have been reported to achieve those four properties, including self-assembly, electrospinning, polymer imprinting, plasma-treated surfaces, lithography, colloidal template technique, laser micromachining, and so on.[1–9,53–55] For instance, Mazur et al. and Stratakis et al., respectively, obtained an excellent superhydrophobic Si surface by femtosecond laser irradiation under reactive gas (SF6) atmosphere.[12,56] These surfaces were composed of microscale conical features with nanoscale protrusion decoration, which could quantitatively mimic both the structure and the water-repellent characteristic of a natural lotus leaf. Jiang et al. prepared a superhydrophobic aligned polystyrene nanotube layer, and obtained a controllable transition between low adhesive rolling and high adhesive pinning states.[15,45] Sun et al. achieved a kind of artificial rice leaves by combing micro/nanostructures and macrogrooves produced by photolithography, polydimethylsiloxane (PDMS) imprint lithography, and micro/nanostructure coating.[23] The reproduced three-level hierarchical surface successfully mimicked the anisotropic sliding ability of the rice leaf. Chen et al. realized an anisotropic wetting property by restricting a droplet on an unstructured Si hydrophobic domain between two superhydrophobic strips fabricated by a femtosecond laser.[32] Although the above mentioned methods can realize various wettabilities, one or two typical aspects of wettability can be just achieved. For obtaining multifunctional applications, a simple way to simultaneously achieve superhydrophobicity, controllable water adhesion, anisotropic sliding, and anisotropic wetting only by adjusting a single parameter has not been reported until now.

In this paper, we report a simple one-step method to generate a line-patterned structure on PDMS surface by a femtosecond laser. The microstructure can be tuned by adjusting the period (D) of the microgroove arrays which are generated by a line-by-line femtosecond laser scanning process. We systematically investigated the relations of the CAs and SAs along the directions parallel to and perpendicular to the microgrooves vs. the D. The results show that superhydrophobicity, controllable water adhesion, anisotropic sliding, and anisotropic wetting can be achieved by the femtosecond-laser-induced line-patterned surfaces with different D. Besides the classical principle, some new viewpoints are introduced to explain our experimental results, such as point contact for self-cleaning effect, and capillary effect in open microgrooves for anisotropic wetting.

2 Experimental

PDMS has many advantages to realize various wettabilities, such as intrinsic hydrophobicity, flexibility, biocompatibility, optical transparency, thermal stability and nontoxicity. In this experiment, the PDMS thin films were prepared from solidifying a 10 : 1 mixture (by weight) of pre-polymer (DC-184A, Dow Corning Corporation) and curing agent (DC-184B, Dow Corning Corporation) in an oven at 100 °C for 2 h. The thickness of the PDMS samples was about 1 mm. The microscale line-patterned structures were achieved by femtosecond laser scanning in air atmosphere on flat PDMS surfaces. The details of the experimental setup and the scanning method were represented by our previous work.[17,19,32,33,57] The PDMS samples were line-by-line

scanned by a 50 fs regenerative amplified Ti:sapphire laser system (Coherent Libra-usp-he) at the center wavelength of 800 nm with a repetition rate of 1 kHz. The laser beam was focused with an objective lens (10×, NA = 0.30, Nikon) on the samples. Each sample was fabricated with a constant average power of 30 mW (energy/pulse of 30 μJ) at a scanning speed of 4 mm s^{-1}. The period or average distance (D) of the adjacent microgrooves was tuned by the interval of adjacent scanning lines. After laser irradiation, the as-prepared samples were cleaned with acetone, alcohol and deionized water in an ultrasonic bath for 10 min, respectively.

The morphology of the as-prepared surfaces was characterized by a JSM-7000F scanning electron microscopy (SEM, JEOL, Japan). The 3D and cross-sectional profiles of the line-patterned surfaces were investigated on a LEXT-OLS4000 laser confocal microscope (Olympus, Japan). The contact angle and the sliding angle of a 7 μl water droplet on the surface were measured by a JC2000D contact-angle system (POWEREACH, China), using a sessile drop method. The average CA and SA values were obtained by measuring the same samples in at least five different positions. The CAs (SAs) measured perpendicular to and parallel to the direction of the microgrooves, respectively, defined as CA$_\perp$ and CA$_\parallel$ (SA$_\perp$ and SA$_\parallel$). The self-cleaning experiment was performed by placing a water droplet to roll across a slightly tilted structured surface ($D = 10$ μm) which was equally strewed with graphite powder. The droplet transfer ability was investigated by the contact-angle system and a charge-coupled device (CCD) camera system to take photographs at 25 frames per second.

3 Results and discussion

3.1 Morphology of structured surfaces

Fig. 1a–c show typical SEM images of the femtosecond laser scanned PDMS surfaces, which are composed of periodic microgrooves. As shown in Fig. 2a, the width and depth of the femtosecond-laser-induced microgrooves are about 12.17 and 8.57 μm, respectively. The magnified SEM images show that the inside wall and the outer rim of the microgrooves are randomly decorated with many irregular particles with size of several nanometers to nearly a micrometer (inset of Fig. 1a–c). The micro/nanoscale hierarchical rough structure was produced during femtosecond laser ablation. With a line-by-line scanning process, the periodic microgrooves were rapidly generated, forming a line-patterned structure. As the D decreases, the femtosecond-laser-induced microgrooves get close to each other (Fig. 1a–c). When D is equal to or smaller than 10 μm, the basic line-patterned structure will be destroyed and a new kind of homogeneous rough surface will be formed due to the adjacent microgrooves with a strong overlap (Fig. 1d). The three-dimensional (3D) and cross-sectional profiles of the femtosecond-laser-induced line-patterned surfaces were also investigated using a laser confocal scanning microscope and the results are shown in Fig. 2. The SEM images and 3D profiles all indicate that the as-prepared line-patterned surfaces are uniform and well-patterned.
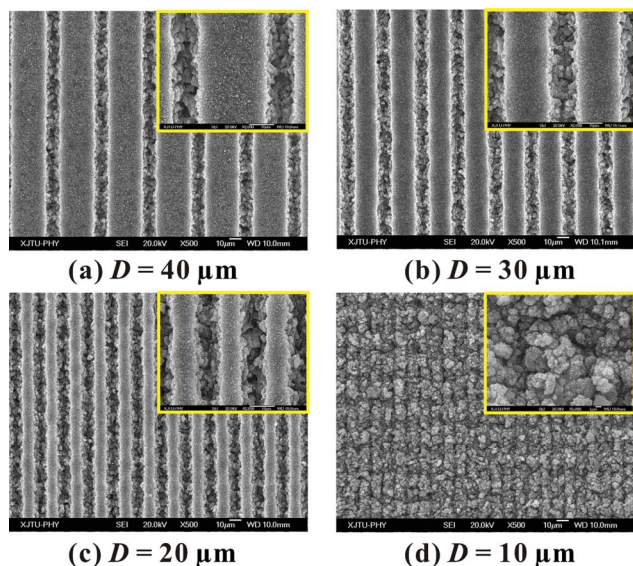
5500 | J. Mater. Chem. A, 2014, **2**, 5499–5507

This journal is © The Royal Society of Chemistry 2014

Fig. 1 SEM images of various femtosecond-laser-induced line-patterned surfaces with different period (D): (a) $D = 40$ μm; (b) $D = 30$ μm; (c) $D = 20$ μm; (d) $D = 10$ μm. The insets are corresponding magnified SEM images.
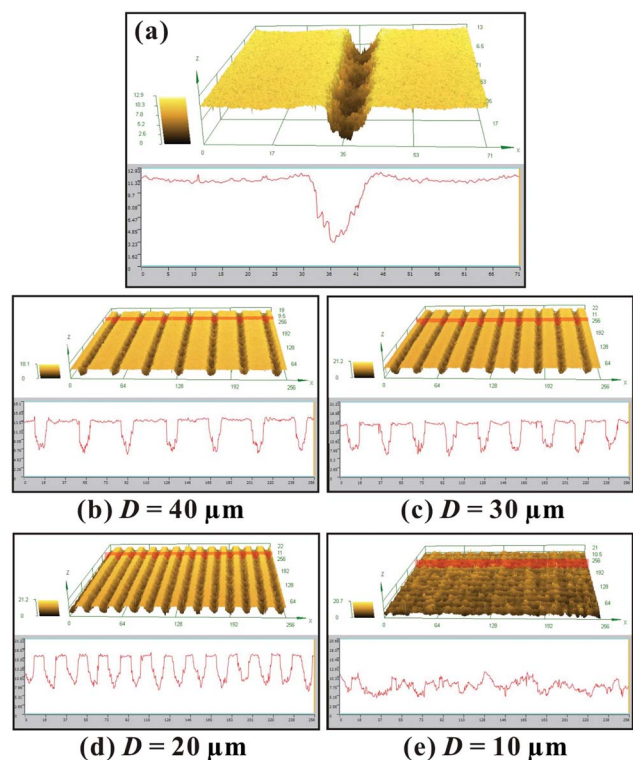

Fig. 2 3D and cross-sectional profiles of the femtosecond-laser-induced line-patterned surfaces. (a) A single microgroove fabricated by femtosecond laser scanning at laser power of 30 mW and speed of 4 mm s^{-1}. (b–e) The as-prepared line-patterned surfaces with different periods (D): (b) $D = 40$ μm; (c) $D = 30$ μm; (d) $D = 20$ μm; (e) $D = 10$ μm.

3.2 Superhydrophobicity

The period of the line-patterned PDMS surfaces, which is the most crucial structure parameter, has an important effect on the water CA/SA of the as-prepared surfaces. In order to evaluate the relationship between D and the surface wettability, PDMS surfaces with different D were selected and compared, as shown in Fig. 3. When D is no more than 10 μm, the femtosecond laser scanning process will produce an entirely uniform micro/nano hierarchical structure (Fig. 1d). The value of static CA on this entire laser-induced surface is as high as $157.5° \pm 1°$ (Fig. 4a), even without any modification by materials of low surface energy. In this case, the superhydrophobicity can be explained by Cassie's theory.[58] The water droplet is suspended by the gas layer trapped at the micro- and nanoscale structures, and only contacts the peak of the micro/nanoscale hierarchical surface. The contact area between the surface and the droplet is so small that the droplet almost has no wetting of the space between the rough structures. When the D is larger than 10 μm, the as-prepared surface is an anisotropic structure, resulting in different CA values measured parallel to or perpendicular to the microgroove arrays. With the perpendicular direction, for example, the $CA_\perp$ slowly decreases from $157.5 \pm 1°$ to $157 \pm 1°$, $156.1 \pm 1°$, $152 \pm 1°$, $152 \pm 2°$, $151.4 \pm 2°$ and then to $150 \pm 2.5°$ as D increases from 10 to 40 μm, as shown in Fig. 3 and 4. The decline of $CA_\perp$ is caused by the decrease of the surface roughness because the fraction of the flat non-structured domain rises with D increasing. It can be clearly seen that the as-prepared surfaces show superhydrophobicity with $CA_\perp$ stabilizing above $150°$ when D is no more than 40 μm in the perpendicular direction. Similarly, superhydrophobicity also can be obtained with D less than 25 μm in the parallel direction (Fig. 3 and 4a–c).

The self-cleaning phenomenon of superhydrophobic surfaces has been the subject of considerable scientific interest over the past two decades.[1–9] The self-cleaning performance of the highly superhydrophobic surface ($D = 10$ μm) was investigated, as shown in Fig. 5. Firstly, graphite powder as pollutant or dirt was deliberately spread on the slightly tilted superhydrophobic surface (Fig. 5a). And then a water droplet was placed on the contaminated surface to roll off freely. During the sliding process, the contaminant powder was immediately picked up and carried away by the water droplet, leaving behind a clear path (Fig. 5b). This experiment indicates that the superhydrophobic surface fabricated by a femtosecond laser has a similar self-cleaning effect of the lotus leaf. The generation mechanism of the self-cleaning effect is revealed in Fig. 5c. As compared with a general surface, the water droplet on a superhydrophobic surface shows a quasi-spherical shape. When the surface is tilted to a certain angle, the water droplet rolls off the surface easily and picks up foreign dirt particles at the same time, this is considering the fact that most dust shows relatively strong adherence to water in comparison to a solid surface.[34] On the other hand, the pollutant only comes to contact with the peak of the micro/nanoscale hierarchical surface, resulting in a smaller van der Waals force between the pollutant and the superhydrophobic surface than the general surface because it is a point contact, not a surface contact (Fig. 5c). The former reason is well-known, but the latter reason has been neglected. Moreover, such self-cleaning ability could be repeated numerous number of times for the stability and intrinsic hydrophobicity of PDMS.
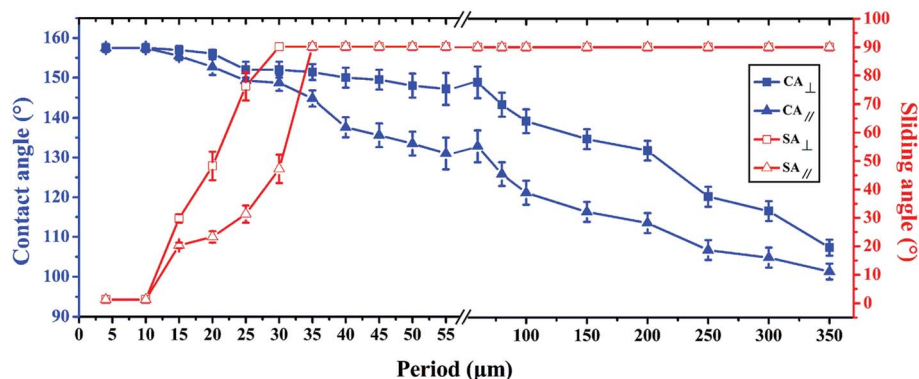
Fig. 3 Relationships between the period of the line-patterned surfaces and the CA (left)/SA (right), respectively.

3.3 Controllable water adhesion

Water adhesion, which is an important property of a solid surface, can be accurately assessed by the sliding behavior of a water droplet. In the case of perpendicular direction, the $SA_\perp$ increases slowly at first and the water droplet can move very easily with the surfaces being only slightly tilted or shaken when D is no more than 10 μm. However, with D increasing from 10 to 30 μm, the $SA_\perp$ gradually increases from $1 \pm 0°$ to $29.5 \pm 1.5°$, $48 \pm 3°$, $76 \pm 4°$ and then to $90°$ that the water droplet does not slide down even when the as-prepared surface is vertical or turned upside down, showing controllable water adhesion (Fig. 3 and movies 1–5 of the ESI†). Finally, the water droplet is firmly pinned on the as-prepared surfaces without any

movement at any tilted angle when D is greater than 30 μm. For the parallel direction, this controllability of water adhesion is equally valid (red hollow triangle in Fig. 3).

The modulation of the adhesion of these surfaces can be ascribed to the change in the area fraction of laser structured and non-structured domains. Based on the above, the femto-second laser structured domain shows superhydrophobicity with ultralow water adhesion for its hierarchical rough structure. On the contrary, the droplet will completely wet the non-irradiated flat surface according to the Young contact model.[9] As a result, the non-structured flat PDMS shows ordinary hydrophobicity with ultrahigh water adhesion because a large contact area results in a greater van der Waals force. With D
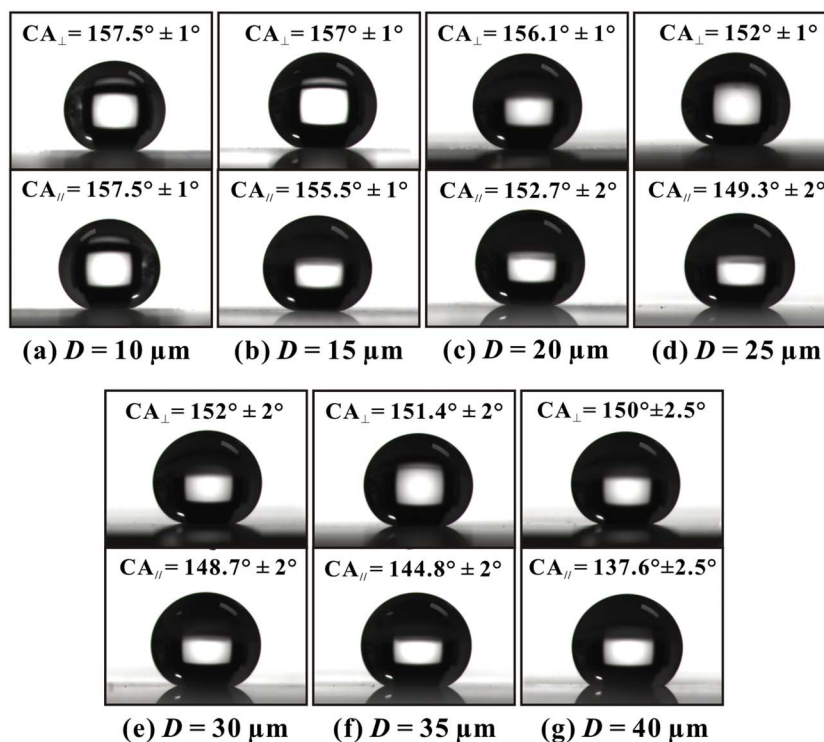

Fig. 4 Images of water droplet shape in two views (perpendicular ($CA_\perp$) to and parallel ($CA_\parallel$) to the direction of the microgrooves) on the surfaces with period (D) from 10 to 40 μm.

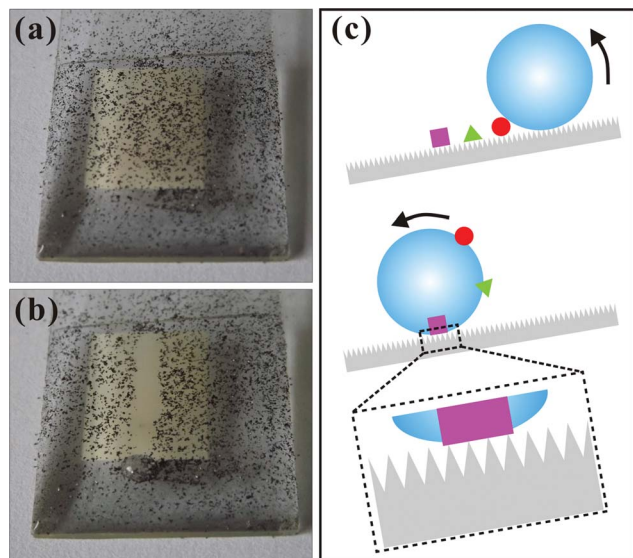**Fig. 5** Self-cleaning effect of the as-prepared superhydrophobic surface with D of 10 μm. (a) Graphite power spreading on the surface. (b) A water droplet rolling through the surface. (c) Schematic depicting the motion of a liquid droplet on an inclined superhydrophobic substratum covered with "dirt".

Fig. 6 Transfer process of a 7 μl water droplet from the A-surface to the C-surface using the B-surface. Surfaces of A, B, and C were as-prepared line-patterned surfaces with D of 10, 30, and 20 μm, respectively.

increasing, the area fraction of the non-structured flat domain increases as well as the water adhesion or SA.

The as-prepared surfaces with controllable adhesion have important potential application in the manipulation of water microdroplets/fluid. As an example, Fig. 6 shows the process of transferring a 7 μl water droplet (movie 6 of the ESI†). A water droplet was initially placed on a superhydrophobic surface (surface of A) with ultralow water adhesion (Step 1). Next, an ultrahigh adhesive superhydrophobic surface (surface of B) was lowered down until it contacted the water droplet (Step 2). By lifting the B-surface up, the water droplet was completely adhered to the B-surface due to the stronger water adhesive force and transferred from A-surface to B-surface (Step 3). Then, the B-surface was moved to another location above the C-surface which had higher water adhesion than A-surface (Step 4). And the B-surface was lowered down again until the hanging droplet contacted with the C-surface (Step 5). Finally, lifting the B-surface up, the water droplet was detached from the B-surface and transferred to the C-surface (Step 6) because the adhesive force between the droplet and the B-surface was less than the resultant force of the gravity of droplet and the adhesive force between droplet and C-surface. In this way, the water droplet was moved from the A-surface to the C-surface using the B-surface. The droplet transfer ability has some wider applications such as drug delivery and component site-oriented release.[22,59]

3.4 Anisotropic sliding

To investigate the directional control of the water-sliding ability, we measured the perpendicular and parallel sliding angles of the line-patterned surfaces. Fig. 7 shows the time sequences of snapshots of a water droplet rolling on the as-prepared surface with D of 25 μm along the parallel and perpendic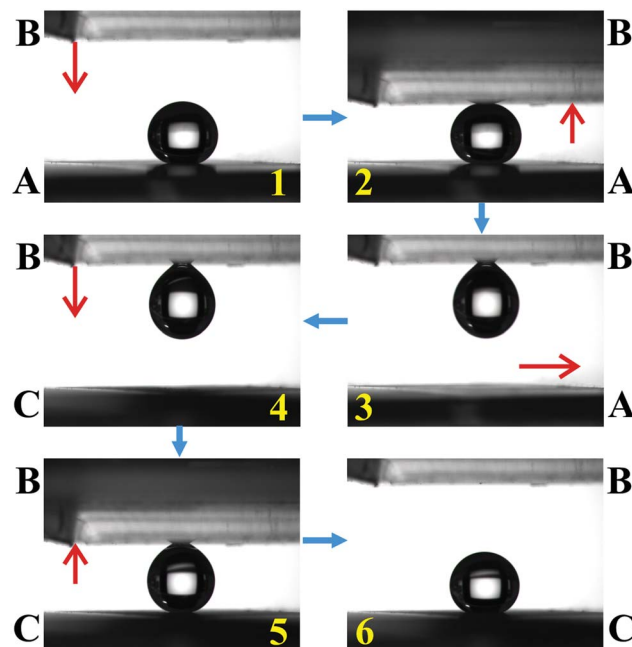ular directions. The measured $SA_{\parallel}$ and $SA_{\perp}$ are $31 \pm 3°$ and $76 \pm 5°$, respectively (movies 7 and 4 of the ESI†). The sliding anisotropy ($SA_{\triangle} = SA_{\perp} - SA_{\parallel}$) is about 45°, which is greater than that of a natural rice leaf (6°). The relationship between the anisotropic sliding and D of the microgrooves was systematically investigated, as shown in Fig. 3. The measurement shows that SAs in the parallel direction were consistently smaller than those in the perpendicular direction in a wide range of D between 10 and 35 μm, indicating that the droplet is easier to roll along the microgrooves. Moreover, the obtained anisotropic sliding is controllable and anisotropy can be tuned from 0 to 45° by adjusting the parameter D because the perpendicular and parallel SAs depend on D.

The anisotropic structure of microgroove arrays is the determining factor in the anisotropic sliding ability.[23–26] The sliding of a water droplet on a solid surface is known to be governed by the movement of the three-phase (solid–water–air) contact line (TCL) toward the sliding direction.[21,60] For groove-like structures, the sliding behavior of water droplets depends on the length and continuity of the TCL on the surface. A continuous short TCL is preferable for a surface with an excellent water-shedding property.[60] Fig. 8 shows the shape and length of the TCL for line-patterned structures. It is clearly shown that the TCL is continuous along the parallel direction of the surface with aligned microgrooves. However, for the perpendicular direction, the TCL is discontinuous, and the length of the TCL is longer than that along the parallel direction, giving rise to more pronounced hysteresis effects. Therefore, the $SA_{\parallel}$ is smaller than $SA_{\perp}$, corresponding to that of the energy gap for the movement of the TCL in the sliding direction.
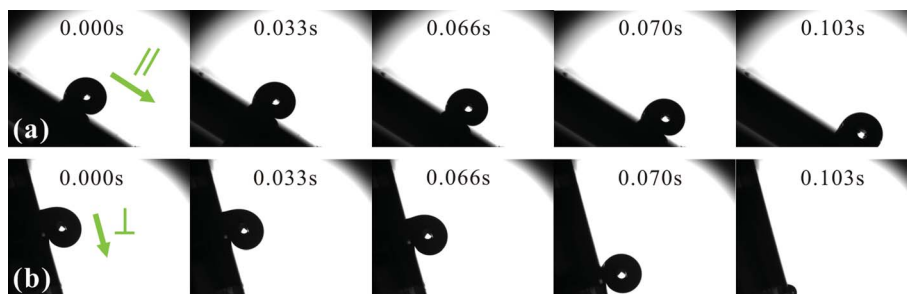
Fig. 7 Time sequences of snapshots of a water droplet rolling on the as-prepared surface with D of 25 μm along the parallel and perpendicular directions. The as-prepared surface in (a) and (b) is tilted 31 and 76°, respectively.
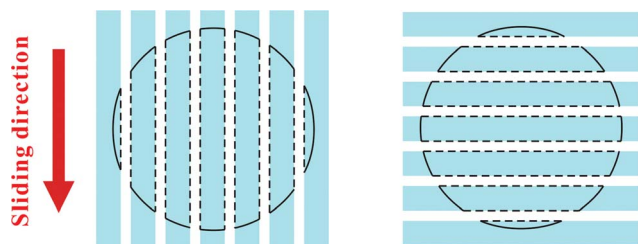

Fig. 8 Schematic illustration of the three-phase contact line from the top view (cyan, flat PDMS parts; white, microgroove parts; circle, contact part of water and solid surface). (a) Sliding in parallel direction of the line-patterned structure; (b) sliding in perpendicular direction of the line-patterned structure.

3.5 Anisotropic wetting

The contact angles along various directions are different on anisotropic microstructures, and the droplet shape is strongly affected by the presence of the oriented microfeatures.[27–33] Generally, the perpendicular and parallel CAs were measured to characterize the anisotropy degree of the groove-like surfaces. Fig. 9a shows an aerial view photograph of a water droplet on the as-prepared surface. The droplet is elongated and the contact line deviates from an ideal circle and becomes stretched along the microgrooves. The superficial morphology therefore induces a preferential liquid imbibition along the microgrooves and liquid pinning in the perpendicular direction. Fig. 9b and c reveal the shapes of a water droplet on the as-prepared surface with $D = 150$ μm along the parallel and perpendicular directions, respectively. The $CA_{\parallel}$ is $116.5 \pm 2.5°$, whereas the $CA_{\perp}$ is $134.8 \pm 2.5°$. The measured degree of wetting anisotropy, defined as the difference of the CA values for the two directions $CA_{\triangle} = CA_{\perp} - CA_{\parallel}$, is about 18.3°. Furthermore, to explore the underlying mechanism of anisotropic wetting behavior, we systematically investigated the water droplet shapes and CAs in the perpendicular and parallel views on the laser-induced line-patterned surfaces with different D from 10–350 μm, as shown in Fig. 3. Although $CA_{\perp}$ and $CA_{\parallel}$ have similar change trends, $CA_{\perp}$ is consistently larger than $CA_{\parallel}$. Fig. 9d shows the function of wetting anisotropy, $CA_{\triangle}$, against the period of line-patterned surfaces, D. With D increasing, $CA_{\triangle}$ initially increases because the anisotropic structure becomes more and more obvious. After reaching the largest value (about 18.3°), $CA_{\triangle}$ decreases gradually for a flat PDMS domain becoming larger.

From the comparison and analysis, we can deduce some main factors of the forming anisotropic wetting phenomenon. First, a lot of recent research has demonstrated that the capillary effect in open microgrooves plays a dominant role in directional guiding of the liquid.[61–68] The water droplet may partly dive into the laser-induced microgrooves, and enhances the directional spreading of the water droplet along the grooves for the capillary action (Fig. 10a). This process can be directly
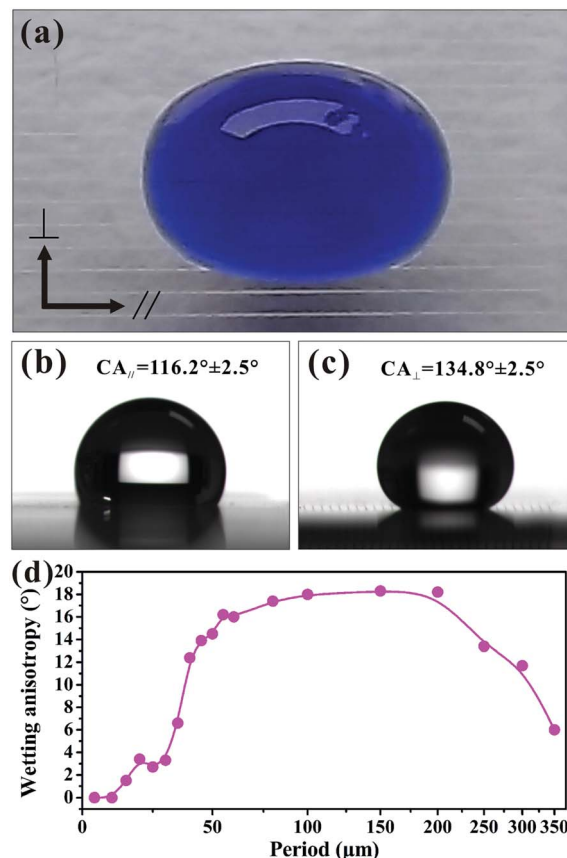

Fig. 9 Anisotropic wetting of the line-patterned surfaces. (a) Optical micrograph of a blue-colored water droplet on the patterned as-prepared surface, revealing an elongated shape. (b and c) Images of a water droplet shape for the parallel (b) and perpendicular (c) directions. (d) Wetting anisotropy as a function against the period (D) of microgroove arrays.

5504 | J. Mater. Chem. A, 2014, 2, 5499–5507

This journal is © The Royal Society of Chemistry 2014

observed, as shown in Fig. 10b and movie 8 of the ESI.† When the droplet contacted the line-patterned surface, some air bubbles would appear between the surface and water. The air bubbles mainly came from the air in the microgrooves which was pushed out during the water droplet diving into. The centre of the droplet went dark as a function of time, which means that the droplet became gradually thicker along the parallel direction, that is, the droplet was elongated along the microgrooves. Second, an energy barrier can form between adjacent different chemical domains or morphology with different apparent surface free energy.[29,30,32] A droplet on the laser irradiated domain is in unstable state, the droplet can easily roll to other places as the surface is disturbed slightly. On the other hand, the droplet can stick on the flat PDMS without any movement at any tilted angle, representing a steady state. In general, the unstable state means that the object is in the highest energy, whereas the steady state stands for a lower energy. Therefore, according to Gibbs' criterion, the droplet needs to overcome the energy barrier between the flat PDMS domain (non-irradiated area between microgrooves) and laser-induced microgroove when it spread from the flat PDMS domain to a laser-induced microgroove. The flat PDMS domain first contacts the droplet and generates strong attraction, inducing the droplet to extend along the microgrooves, while the higher hydrophobic microgrooves prevent water from spreading in the perpendicular direction. Moreover, the droplet has a continuous TCL along the microgrooves and can also facilitate the spreading and moving of the droplet.[60] As a result, the contact angles in the perpendicular direction are higher than those in the parallel direction.

4 Conclusions

In conclusion, a method to realize superhydrophobicity, controllable water adhesion, anisotropic sliding, and anisotropic wetting by a femtosecond-laser-induced line-patterned PDMS surface is demonstrated. By varying the period (D) of the microgroove arrays, both static and dynamic wettability can be tuned. The as-prepared surfaces show superhydrophobicity with D being no more than 40 μm in the perpendicular direction or less than 25 μm in the parallel direction. Compared with a traditional superhydrophobic surface, the adhesion of the as-prepared surfaces can be controlled from ultralow to ultrahigh by adjusting D from 10 to 35 μm along the perpendicular direction (or 10 to 30 μm along the parallel direction). In addition, anisotropic sliding and anisotropic wetting also can be achieved, and the maximum values of anisotropy are about 45 and 18.3°, respectively. The method is very simple, but we believe that the developed approach will have important potential applications for droplets/fluid manipulation, microfluidics, fluid microreactors, biomedicine, chemical and biological sensing, fuel cells, and catalysts.

Acknowledgements

References

1 F. Xia and L. Jiang, *Adv. Mater.*, 2008, **20**, 2842–2858.
2 T. L. Sun and G. Y. Qing, *Adv. Mater.*, 2011, **23**, H57–H77.
3 K. S. Liu and L. Jiang, *Annu. Rev. Mater. Res.*, 2012, **42**, 231–263.
4 K. S. Liu and L. Jiang, *Nano Today*, 2011, **6**, 155–175.
5 X. Yao, Y. L. Song and L. Jiang, *Adv. Mater.*, 2011, **23**, 719–734.
6 F. Chen, D. S. Zhang, Q. Yang, J. L. Yong, G. Q. Du, J. H. Si, F. Yun and X. Hou, *ACS Appl. Mater. Interfaces*, 2013, **5**, 6777–6792.
7 Y. L. Zhang, H. Xia, E. Kim and H. B. Sun, *Soft Matter*, 2012, **8**, 11217–11231.
8 Y. L. Zhang, Q. D. Chen, Z. Jin, E. Kim and H. B. Sun, *Nanoscale*, 2012, **4**, 4858–4869.
9 Y. B. Zhang, Y. Chen, L. Shi, J. Li and Z. G. Guo, *J. Mater. Chem.*, 2012, **22**, 799–815.
10 X. Deng, L. Mammen, Y. Zhao, P. Lellig, K. Müllen, C. Li, H. J. Butt and D. Vollmer, *Adv. Mater.*, 2011, **23**, 2962–2965.
11 Y. Li, L. Li and J. Q. Sun, *Angew. Chem.*, 2010, **122**, 6265–6269.
12 V. Zorba, E. Stratakis, M. Barberoglou, E. Spanakis, P. Tzanetakis, S. H. anastasiadis and C. Fotakis, *Adv. Mater.*, 2008, **20**, 4049–4054.
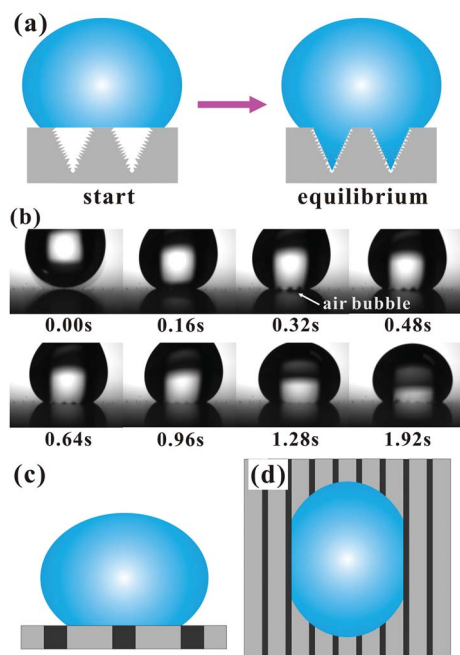
Fig. 10 The underlying reasons for anisotropic wetting. (a) Schematic illustration of water droplet partly diving into the laser-induced microgrooves. (b) Time sequences of snapshots of a water droplet contacting the as-prepared surface along the parallel direction. (c and d) Side and top views of schematic illustration of a water droplet being restrained by an energy barrier between laser-induced microgrooves (black parts) and non-structured flat domains (grey parts).

13 N. R. Chiou, C. Lu, J. Guan, L. J. Lee and A. J. Epstein, *Nature*, 2007, **2**, 354–357.

14 J. L. Yong, Q. Yang, F. Chen, D. S. Zhang, H. Bian, Y. Ou, J. H. Si, G. Q. Du and X. Hou, *Appl. Phys. A: Mater. Sci. Process.*, 2013, **111**, 243–249.

15 Y. K. Lai, X. F. Gao, H. F. Zhuang, J. Y. Huang, C. J. Lin and L. Jiang, *Adv. Mater.*, 2009, **21**, 3799–3803.

16 Z. J. Cheng, M. Du, H. Lai, N. Q. Zhang and K. N. Sun, *Nanoscale*, 2013, **5**, 2776–2783.

17 J. L. Yong, F. Chen, Q. Yang, D. S. Zhang, H. Bian, G. Q. Du, J. H. Si, X. W. Meng and X. Hou, *Langmuir*, 2013, **29**, 3274–3279.

18 J. L. Yong, Q. Yang, F. Chen, D. S. Zhang, G. Q. Du, H. Bian, J. H. Si, F. Yun and X. Hou, *Appl. Surf. Sci.*, 2014, **288**, 579–583.

19 D. S. Zhang, F. Chen, Q. Yang, J. L. Yong, H. Bian, Y. Ou, J. H. Si, X. W. Meng and X. Hou, *ACS Appl. Mater. Interfaces*, 2012, **4**, 4905–4912.

20 J. Li, X. H. Liu, Y. P. Ye, H. D. Zhou and J. M. Chen, *J. Phys. Chem.C*, 2011, **115**, 4726–4729.

21 X. D. Zhao, H. M. Fan, X. Y. Liu, H. H. Pan and H. Y. Xu, *Langmuir*, 2011, **27**, 3224–3228.

22 M. Wang, C. Chen, J. P. Ma and J. Xu, *J. Mater. Chem.*, 2011, **21**, 6962–6967.

23 D. Wu, J. N. Wang, S. Z. Wu, Q. D. Chen, S. Zhao, H. Zhang, H. B. Sun and L. Jiang, *Adv. Funct. Mater.*, 2011, **21**, 2927–2932.

24 Y. M. Zheng, X. F. Gao and L. Jiang, *Soft Matter*, 2007, **3**, 178–182.

25 N. A. Malvadkar, M. J. Hancock, K. Sekeroglu, W. J. Dressick and M. C. Demirel, *Nat. Mater.*, 2010, **9**, 1023–1028.

26 M. J. Hancock, K. Sekeroglu and M. C. Demirel, *Adv. Funct. Mater.*, 2012, **22**, 2223–2234.

27 M. Gleiche, L. F. Chi and H. Fuchs, *Nature*, 2000, **403**, 173–175.

28 S. Z. Wu, D. Wu, J. Yao, Q. D. Chen, J. N. Wang, L. G. Niu, H. H. Fang and H. B. Sun, *Langmuir*, 2010, **26**, 12012–12016.

29 J. Y. Chung, J. P. Youngblood and C. M. Stafford, *Soft Matter*, 2007, **3**, 1163–1169.

30 E. Mele, S. Girardo and D. Pisignano, *Langmuir*, 2012, **28**, 5312–5317.

31 S. G. Park, J. H. Moon, H. C. Jeon and S. M. Yang, *Soft Matter*, 2012, **8**, 4567–4570.

32 F. Chen, D. S. Zhang, Q. Yang, X. H. Wang, B. J. Dai, X. M. Li, X. Q. Hao, Y. C. Ding, J. H. Si and X. Hou, *Langmuir*, 2011, **27**, 359–365.

33 D. S. Zhang, F. Chen, Q. Yang, J. H. Si and X. Hou, *Soft Matter*, 2011, **7**, 8337–8342.

34 W. Barthlott and C. Neinhuis, *Planta*, 1997, **202**, 1–8.

35 T. K. Wong, S. H. Kang, S. K. Y. Tang, E. J. Smythe, B. D. Hatton, A. Grinthal and J. Aizenberg, *Nature*, 2011, **477**, 443–446.

36 W. Barthlott, T. Schimmel, S. Wiersch, K. Koch, M. Brede, M. Barczewski, S. Walheim, A. Weis, A. Kaltenmaier, A. Leder and H. F. Bohn, *Adv. Mater.*, 2010, **22**, 2325–2328.

37 X. F. Gao, X. Yan, X. Yao, L. Xu, K. Zhang, J. H. Zhang, B. Yang and L. Jiang, *Adv. Mater.*, 2007, **19**, 2213–2217.

38 M. Motornov, R. Sheparovych, R. Lupitskyy, E. MacWilliams and S. Minko, *Adv. Mater.*, 2008, **20**, 200–205.

39 G. McHale, N. J. Shirtcliffe, C. R. Evans and M. I. Newton, *Appl. Phys. Lett.*, 2009, **94**, 064104.

40 Y. K. Lai, Y. X. Tang, J. J. Gong, D. G. Gong, L. F. Chi, C. J. Lin and Z. Chen, *J. Mater. Chem.*, 2012, **22**, 7420–7426.

41 N. J. Shirtcliffe, G. McHale, M. I. Newton and Y. Zhang, *ACS Appl. Mater. Interfaces*, 2009, **1**, 1316–1323.

42 L. Feng, Y. N. Zhang, J. M. Xi, Y. Zhu, N. Wang, F. Xia and L. Jiang, *Langmuir*, 2008, **24**, 4114–4119.

43 X. Hong, X. F. Gao and L. Jiang, *J. Am. Chem. Soc.*, 2007, **129**, 1478–1479.

44 D. Wu, S. Z. Wu, Q. D. Chen, Y. L. Zhang, J. Yao, X. Yao, L. G. Niu, J. N. Wang, L. Jiang and H. B. Sun, *Adv. Mater.*, 2011, **23**, 545–549.

45 M. H. Jin, X. J. Feng, L. Feng, T. L. Sun, J. Zhai, T. J. Li and L. Jiang, *Adv. Mater.*, 2005, **17**, 1977–1981.

46 L. Feng, S. H. Li, Y. S. Li, H. J. Li, L. J. Zhang, J. Zhai, Y. L. Song, B. Q. Liu, L. Jiang and D. B. Zhu, *Adv. Mater.*, 2002, **14**, 1857–1860.

47 B. P. Casavant, E. Berthier, A. B. Theberge, J. Berthier, S. I. Montanez-Sauri, L. L. Bischel, K. Brakke, C. J. Hedman, W. Bushman, N. P. Keller and D. J. Beebe, *Proc. Natl. Acad. Sci. U. S. A.*, 2013, **110**, 10111–10116.

48 H. Mertaniemi, V. Jokinen, L. Sainiemi, S. Franssila, A. Marmur, O. Ikkala and R. H. A. Ras, *Adv. Mater.*, 2011, **23**, 2911–2914.

49 H. F. Bohn and W. Federle, *Proc. Natl. Acad. Sci. U. S. A.*, 2004, **101**, 14138–14143.

50 B. Zhao, J. S. Moore and D. J. Beebe, *Science*, 2001, **291**, 1023–1026.

51 S. M. Kim, D. H. Kang, J. H. Koh, H. S. Suh, H. Yoon, K. Y. Suh and K. Char, *Soft Matter*, 2013, **9**, 4145–4149.

52 K. H. Chu, R. Xiao and E. N. Wang, *Nat. Mater.*, 2010, **9**, 413–417.

53 Y. Li, W. P. Cai, B. Q. Cao, G. T. Duan, F. Q. Sun, C. C. Li and L. H. Jia, *Nanotechnology*, 2006, **17**, 238–243.

54 Y. Li, E. J. Lee and S. O. Cho, *J. Phys. Chem. C*, 2007, **111**, 14813–14817.

55 Y. Li, X. J. Huang, S. H. Heo, C. C. Li, Y. K. Choi, W. P. Cai and S. O. Cho, *Langmuir*, 2007, **23**, 2169–2174.

56 T. Baldacchini, J. E. Carey, M. Zhou and E. Mazur, *Langmuir*, 2006, **22**, 4917–4919.

57 J. L. Yong, F. Chen, Q. Yang, G. Q. Du, H. Bian, D. S. Zhang, J. H. Si, F. Yun and X. Hou, *ACS Appl. Mater. Interfaces*, 2013, **5**, 9382–9385.

58 S. T. Wang and L. Jiang, *Adv. Mater.*, 2007, **19**, 3423–3424.

59 J. L. Yong, F. Chen, Q. Yang, D. S. Zhang, G. Q. Du, J. H. Si, F. Yun and X. Hou, *J. Phys. Chem. C*, 2013, **117**, 24907–24912.

60 Z. Yoshimitsu, A. Nakajima, T. Watanabe and K. Hashimoto, *Langmuir*, 2002, **18**, 5818–5822.

61 J. C. Baret and M. M. J. Decré, *Langmuir*, 2007, **23**, 5200–5204.

62 K. Khare, S. Herminghaus, J. C. Baret, B. M. Law, M. Brinkmann and R. Seemann, *Langmuir*, 2007, **23**, 12997–13006.

63 R. R. Rye, J. A. Mann, Jr and F. G. Yost, *Langmuir*, 1996, **12**, 555–565.

64 A. Y. Vorobyev and C. L. Guo, *Appl. Phys. Lett.*, 2009, **94**, 224102.

65 A. Y. Vorobyev and C. L. Guo, *J. Appl. Phys.*, 2010, **108**, 123512.

66 Y. M. Zheng, H. Bai, Z. B. Huang, X. L. Tian, F. Q. Niu, Y. Zhao, J. Zhai and L. Jiang, *Nature*, 2010, **463**, 640–643.

67 J. Ju, H. Bai, Y. M. Zheng, T. Y. Zhao, R. C. Fang and L. Jiang, *Nat. Commun.*, 2012, **3**, 1247.

68 K. Li, J. Ju, Z. X. Xue, J. Ma, L. Feng, S. Guo and L. Jiang, *Nat. Commun.*, 2013, **4**, 2276.